Influence from long-distance transport, local sources and precipitation on black carbon concentrations at a rural background field station in southern Sweden

Kit Ming Yam
Supervisor: Pontus Roldin

LUND
UNIVERSITY

ACADEMIC THESIS
which, for the degree of Bachelor of Meteorology and Biogeophysics, by due permission of the Faculty of Science, Lund University, Sweden, will be examined on Monday 27th May 2019 at the Department of Physics, Sölvegatan 14, Lund.

Abstract

The year 2018 was the first complete year with aerosol observations at the rural background station Hyltemossa in southern Sweden. The aim of this thesis was to analyse and investigate the influence from long-distance transport (LDT) aerosols, local sources and precipitation on the black carbon (BC) mass concentration by utilising the Aethalometer and the HYSPLIT model, which estimated the BC mass concentration ([BC]) and simulated the origin of the LDT air masses to Hyltemossa, respectively. The results were evaluated in terms of the probability distribution and geometric mean of [BC]. They indicate that air masses that contained relatively high [BC] at Hyltemossa station tended to originate from Eastern Europe through LDT air masses. Additionally, the influence from local sources (Øresund) had a statistically significant local contribution to [BC] after eliminating the influence from Eastern Europe. Moreover, the estimated geometric mean of [BC] had a decreasing trend as the accumulated precipitation increased (wet scavenging). In the last section, the local contribution to [BC] at a busy street in Malmö was estimated and compared with the [BC] at Hyltemossa station.

Author's contribution to the thesis

I planned and designed the study together with Pontus Roldin. I analysed the Aethalometer BC data and the HYSPLIT model results and wrote the thesis. I constructed parts of the Matlab code which were used to analyse the Aethalometer and HYSPLIT results.

Contents

1 Introduction

1.1 Atmospheric aerosols and climate

In addition to nitrogen, oxygen, argon, water vapour and carbon dioxide (CO_2), there exists many minute aerosols suspended in the atmosphere that affect the climate on the earth. An aerosol is defined as a suspension of solid or liquid particles in a gas, including both the particles and the suspending gas, which is air for atmospheric aerosols (Hinds, 1999). Atmospheric aerosols can be of natural or anthropogenic origin. They either originate from emissions of particulate matter directly into the atmosphere (primary aerosol particles) or from formation of particulate matter by chemical reactions of gaseous compounds in the atmosphere (secondary aerosol particles) (Bond et al., 2013 and Boucher et al., 2013).

According to the fifth assessment report by the Intergovernmental Panel on Climate Change (IPCC), there are three aerosol effects influencing the climate on the earth: (1) scattering and absorption of the incoming solar radiation by atmospheric aerosols (aerosol–radiation interaction); (2) change in the properties of clouds (aerosol–cloud interaction); (3) reduction of surface albedo when BC is deposited on snow and ice (Myhre et al., 2013). The so-called radiative forcing can be calculated by estimating these effects. It is a radiative perturbation due to the presence of a compound (e.g. BC), which triggers an initial change in radiation balance of the earth–atmospheric system (Jacob, 1999). The radiative forcing gives a quantitative index to estimate and compare the potential of various atmospheric disturbances on the radiation balance and climate on the earth (Jacob, 1999).

1.1.1 BC

BC is an atmospheric aerosol that causes net heating effect on the climate on the earth. BC is classified as carbonaceous aerosol particles that absorb solar radiation and heat the surrounding atmosphere. IPCC has estimated that emissions of BC have a radiative forcing of $+0.64\,\mathrm{W/m^2}$ (with an uncertainty range from $+0.25$ to $+1.1\,\mathrm{W/m^2}$) through aerosol–radiation interactions and BC on snow (Myhre et al., 2013). According to the review by Bond et al. (2013), BC is the second-largest contributor to present-day global warming after CO_2, with an approximated total radiative forcing of $+1.1\,\mathrm{W/m^2}$ (with 90 % uncertainty bounds of $+0.17$ to $+2.1\,\mathrm{W/m^2}$). Moreover, as stated in the results of Hansen and Nazarenko (2004), the effect of BC on snow and ice albedos (1.5 % spectral-mean albedo change over the Arctic, 3 % over the Northern Hemisphere land areas and 0.6 % over

Greenland) generate a mean radiative forcing of $+0.3\,\mathrm{W/m^2}$ in the Northern Hemisphere. The equilibrium temperature change of this radiative forcing is approximately twice as large as for a CO_2 radiative forcing of the same magnitude (Hansen and Nazarenko, 2004).

As a component of fine particulate matter, BC is an air pollutant that harms public health through inhalation of air. Deposition of aerosol particles in the respiratory tract gives rise to the adverse health effects which are mostly cardiovascular and respiratory diseases (Löndahl, 2009). The World Health Organization (WHO) has estimated that air pollution in both cities and rural areas caused 4.2 million premature deaths worldwide in 2016, due to exposure to fine particulate matter (World Health Organization, 2018). As mentioned above, BC is one of the dominant climate forcers and affects public health. For these reasons it is important to monitor [BC] in the atmosphere and to analyse the sources and processes that influence [BC].

BC is formed from incomplete combustions of fossil fuel and biomass. The European emission inventory TNO-MACC_III shows that the main sources of BC in Europe are transport (both on-road and non-road) and residential combustion, accounting for about 84 % of total BC emissions in Europe (Kuenen et al., 2014). By looking at the contribution scales of BC in Europe, most BC emissions in Northern and Eastern Europe originate from residential combustion (approximately 50 %), while that in Central and Southern Europe originate from transport (roughly 59 %) (Kuenen et al., 2014). The majority of emissions from transport are from diesel combustion, and emissions from residential combustion come from wood or other biomass burning for domestic heating.

1.2 HYSPLIT

In order to estimate the origin of LDT aerosol particles in southern Sweden, the Hybrid Single-Particle Lagrangian Integrated Trajectory Model (HYSPLIT), developed by NOAA's Air Resources Laboratory (Stein et al., 2015), is applied within this study. The HYSPLIT calculation method is a hybrid between a Lagrangian approach and an Eulerian methodology as described by Stein et al. (2015). The Lagrangian approach uses a moving frame of reference for the advection and diffusion calculations as the trajectories or aerosol particles move from their initial location; the Eulerian methodology uses a fixed three-dimensional grid as a frame of reference to compute pollutant air concentrations (Stein et al., 2015). In this work only the Lagrangian trajectory model was used for tracking the air mass origin.

1.3 Aethalometer

Aethalometer (model AE33, Magee Scientific) is an instrument for real-time measurement of light absorbing BC aerosol particles in air. It measures the light absorption of BC from the rate of change of light attenuation, and thereby estimates [BC]. The Aethalometer utilises an airflow through a roll of quartz filter tape where the samples are deposited as a spot. Hence, a continuous optical analysis can be carried out, while the samples is being collected. The filter tape only moves forward when the spot has reached a certain amount, which depends on the carbon particulate concentration of the location (Hansen and Schnell, 2005). For BC measurement, an optical measurement is required to give a continuous readout of real-time data. The filter deposition spot is thus illuminated with seven laser diodes of different wavelengths spanning from the near infrared to the near ultraviolet (Magee scientific, 2017).

1.4 Main objectives of this thesis

The overall aim of this bachelor project is to analyse aerosol particle measurement from the first complete year of aerosol particle observations at the new Hyltemossa field station in north Scania (56°6′N, 13°25′E). Using data from the Aethalometer and the HYSPLIT model, we aim to identify episodes with urban influence from several European regions at Hyltemossa field station. This project specifically investigates the influence from LDT aerosols, local sources and precipitation on [BC] during 2018.

2 Methods

2.1 HYSPLIT data processing

The Global Data Assimilation System (GDAS) archived, reanalysed meteorological data (1° by 1° grid/scale) were used as an input to the HYSPLIT model. A large data set consisting of air mass trajectories (i.e. latitude and longitude of the traced air masses), altitudes and accumulated precipitation was obtained through the operation of the HYSPLIT model. The air mass trajectories were calculated 7-days backward in time, arriving once every hour at Hyltemossa for the whole year of 2018. All backward trajectories were started 100 m above ground at Hyltemossa field station. Furthermore, the accumulated precipitation from the GDAS data along the trajectories during the last 6, 12, 24 and 48 h before arrival at Hyltemossa were used to evaluate the influence of precipitation on [BC].

A similar approach was used by Martinsson et al. (2017).

Before performing further analysis on the measured [BC], it is important to clarify how the different source regions of LDT BC were defined. Table 1 shows the examined European regions according to how they were defined in this study. In the analysis of air mass origins, only the air mass trajectories below 1000 m above ground were considered. This altitude approximately represents the maximum altitude (mixing height) where the air mass composition (in this case [BC]) can be considered to be influenced by emissions at the earth's surface, within the timescale of one day.

Table 1: The maximum and minimum of latitudes and longitudes of the following examined European regions.

	Max lat.	Min lat.	Max long.	Min long.
Øresund (Malmö & Copenhagen)	55°42′N	55°30′N	13°6′E	12°24′E
Northeast (NE)	– –	58°0′N	– –	14°0′E
Northwest (NW)	– –	58°0′N	12°0′E	– –
Southeast (SE)	55°0′N	– –	– –	14°0′E
Southwest (SW)	55°0′N	– –	12°0′E	– –

2.2 [BC] determination based on light absorption measurements

The Aethalometer estimates [BC] in air by measuring the transmission of light through a portion of the sample-laden filter tape acting as a sensing area. This is compared with the transmission through an unloaded portion of the filter tape acting as a reference area (Magee scientific, 2017). Under the irradiation of laser diodes with seven different wavelengths (370, 470, 520, 590, 660, 880 and 950 nm), the instantaneous [BC] is computed from the rate of change of the attenuation of light transmitted through the particle-laden filter (Magee scientific, 2017). Two measurements with different rates of accumulation of the sample are combined mathematically to eliminate a nonlinear relation between the transmission of light and the amount of light absorbed by the sample (loading effect), and provide the compensated particle light absorption from which [BC] can be derived (Magee scientific, 2017). Figure 1 illustrates the basic principle of the Aethalometer measurement technique.

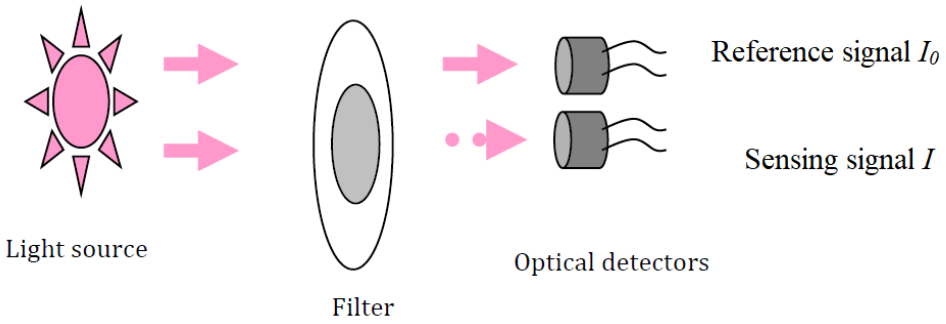

Figure 1: The light absorption measurements are acquired on the filter loaded with aerosols inside the Aethalometer. Adopted and modified from Magee scientific (2017).

The Aethalometer applies the following built-in equations (Magee scientific, 2017) to analyse BC. The optical attenuation ATN is calculated per unit of time:

$$ATN = -100 \cdot \ln\left(I/I_0\right) \tag{1}$$

where I_0 is the reference signal in the reference area and I is the sensing signal in the sensing area. The inflow of air through the filter is

$$F_{in} = F_{out} \cdot (1 - \zeta) \tag{2}$$

where F_{out} is the measured flow and ζ is the leakage factor. The attenuation coefficient is given by

$$b_{atn} = \frac{S \cdot (\Delta ATN/100)}{F_{in}\Delta t} \tag{3}$$

where S is the sensing area and ΔATN is the change of optical attenuation within a time step Δt (Drinovec et al., 2015). The absorption coefficient, in the units of m^{-1}, is then expressed as

$$b_{abs} = \frac{b_{atn}}{C} \tag{4}$$

where C is the multiple scattering parameter that corrects an increased underestimation of the measured aethalometer signals raised by increasing filter loads (Weingartner et al., 2003). Result of Drinovec et al. (2015) shows that the value of C depends on the filter material used, $C_{quartz} = 2.14$ for quartz filter and $C_{TFE} = 1.57$ for tetrafluoroethylene (TFE)-coated glass filter. The measured [BC] can be calculated as

$$[\mathrm{BC}_{\mathrm{measured}}] = \frac{b_{abs}}{\sigma_{air}} \tag{5}$$

where σ_{air} is the mass absorption cross-section of BC as shown in Table 2. σ_{air} denotes

an effective cross-sectional area of BC particles per unit mass of BC. A high value of σ_{air} means that the probability that the BC particles in the air will absorb the incoming light is high, while a low value of σ_{air} means that the probability that the BC particles will absorb the incoming light is low.

Table 2: The mass absorption cross-sections of BC used in calculations, corresponding to seven different wavelengths. Data retrieved from Magee scientific (2017).

Channel	Measurement wavelength (nm)	Mass absorption cross-section σ_{air} (m^2/g)
1	370	18.47
2	470	14.54
3	520	13.14
4	590	11.58
5	660	10.35
6	880	7.77
7	950	7.19

Noteworthy that the absorption coefficient b_{abs} is analogous to the extinction coefficient σ_e of the aerosol for transmitted light through the sample-laden filter in the Lambert-Beer law

$$\frac{I_{tr}}{I_{in}} = e^{-\sigma_e L} \tag{6}$$

where I_{tr}/I_{in} is the ratio of the light intensity traversing the filter to that incident on the filter, and L is the path length of the light beam through the filer and the sample spot on the filter. Both b_{abs} and σ_e represent the fractional loss in signal and intensity per unit path length associated with an elemental thickness dL (Hinds, 1999). The units of σ_e must be m^{-1} such that the exponent of Eq. 6 becomes dimensionless, and it is consistent with the units of b_{abs}.

In order to eliminate the loading effect in the calculations, a compensation parameter k is introduced in the final equation of [BC]:

$$[\mathrm{BC}] = \frac{[\mathrm{BC}_{\mathrm{measured}}]}{1 - k \cdot ATN} \tag{7}$$

By following the user manual of the Aethalometer, model AE33, all measurements of [BC] were obtained from channel 6, which is the defining criterion for reporting [BC] (Magee scientific, 2017). In this work the initial 5 minute resolution observations were averaged to one hour resolution in order to be consistent with the time resolution of the HYSPLIT air mass trajectories.

2.3 Definition of influence in this study

Each one hour average [BC] data point at Hyltemossa corresponds to each one hour average HYSPLIT air mass. In total 8711 measurement data points were analysed for the year 2018, which gives a data coverage of $> 99\,\%$. If an air mass (HYSPLIT air mass trajectory) spends time in a region defined in Table 1 upwind Hyltemossa, the BC in the air mass is considered to be with influence from that region (w.i.f.). Otherwise, the BC in the air mass is considered to be without influence from that region (wo.i.f.). With this approach, it is possible that the same air mass may be influenced by several of the defined source regions in Table 1, at different times upwind Hyltemossa.

2.4 Statistical methods

T-tests were used to investigate if there were any statistically significant differences in the measured [BC] at Hyltemossa station depending on the air mass origin or precipitation intensity upwind Hyltemossa. *T*-test requires a null hypothesis and that the data are normally distributed. The null hypothesis, which is widely used in statistics, proposes that there is no statistically significant difference between two designated populations. For example, if the null hypothesis states that the Aethalometer data (population) come from a normal distribution with a hypothesised mean, the rejection of the null hypothesis implies that there is a significant difference between the population mean and the hypothesised mean. This is specific for the *t*-test function in Matlab, which was used for the analysis. *T*-test in Matlab returns the results in h, p and a confidence interval (CI) of the true population mean. If $h = 0$, this indicates that the null hypothesis cannot be rejected at the $5\,\%$ significance level, whereas $h = 1$ indicates that the null hypothesis can be rejected at the $5\,\%$ significance level. The value of p denotes the significance level, where a small value of p suggests that the null hypothesis can be rejected with large certainty.

3 Results and discussion

3.1 Demonstration of the air mass trajectories

The HYSPLIT model simulates air mass trajectories backward in time. Figure 2 shows an example of the 7-days backward trajectories, where the red and blue lines were representing the trajectories calculated in the morning and evening of the 30th of October, respectively. In this example the air mass trajectories had spent most of the time over NE or SE Europe before arrival at Hyltemossa station.

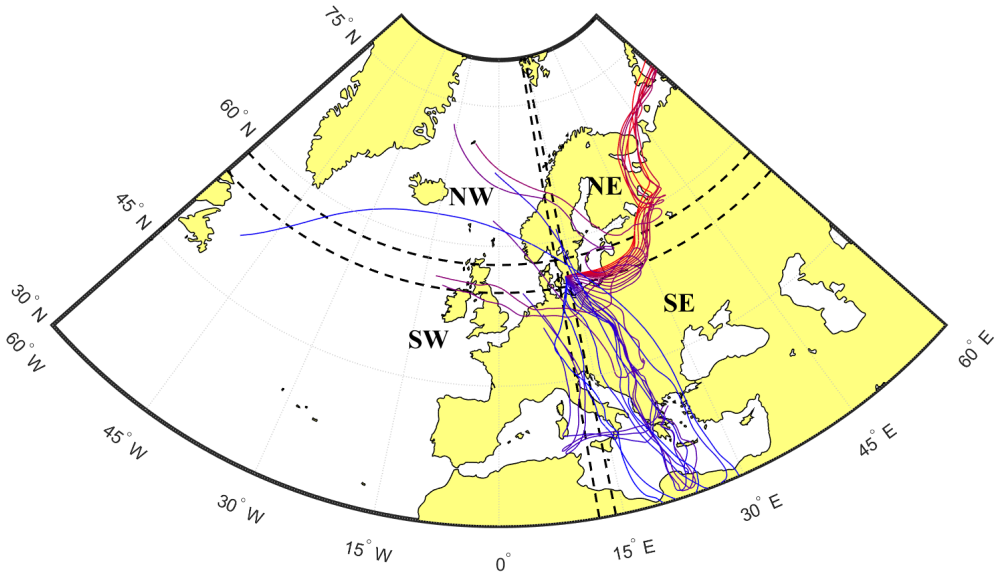

Figure 2: The air mass trajectories had started 7-days before they arrived at Hyltemossa station on 30th of October, 2018, and they were calculated every hour.

3.2 [BC] analysis

3.2.1 Distribution of the Aethalometer data

The frequency distributions of the measurements of [BC] are presented in histogram as shown in Figure 3. Since the raw data measured by the Aethalometer were approximately log-normally distributed (Figure 3a), it was not possible to run the *t*-test under the null hypothesis directly on the raw data. To cope with this problem, we used the natural logarithm (ln) on the measured [BC] (Figure 3b), which appears to be approximately normally distributed. Therefore, it is reasonable to use the *t*-test in order to investigate trends in the geometric mean of [BC] ($[BC]_{GM}$) in later sections.

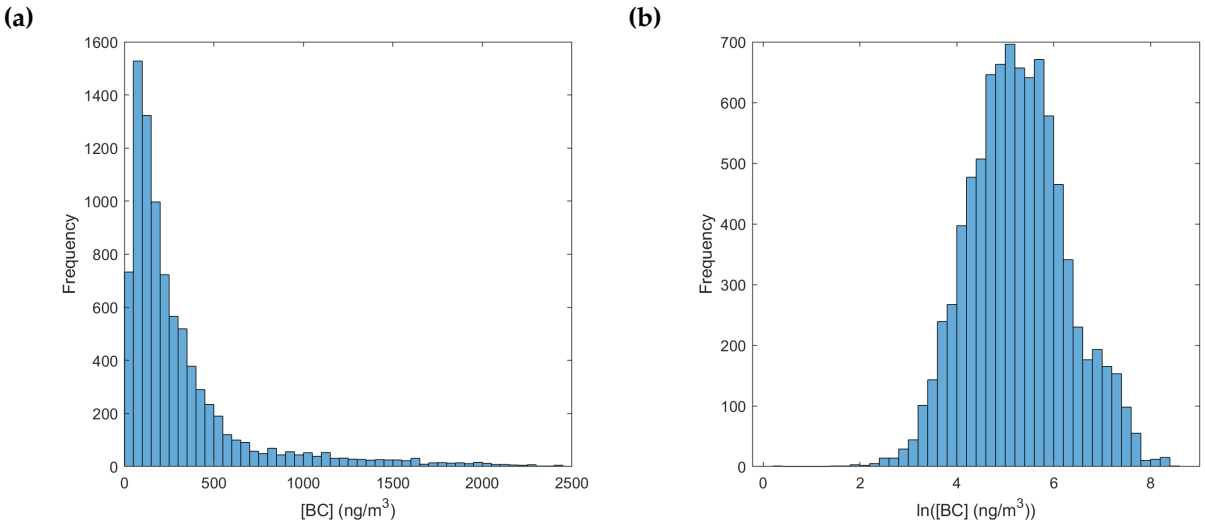

Figure 3: The frequency distributions of **(a)** the [BC] from the Aethalometer data and **(b)** the natural logarithm of the corresponding data.

3.2.2 Influence from different source regions of LDT aerosol particles over Europe

Figure 4 reflects the influence from NE, NW, SE and SW Europe on [BC] at Hyltemossa station through LDT in 2018; it provides the probability distribution in histogram with bin width of 100 ng/m^3. Note that the air masses w.i.f. a specific region does not imply that it excludes the influence from other source regions, thus conditions of the air masses wo.i.f. the examined European regions are also considered. However, we focus on describing conditions of the air masses w.i.f. the examined European regions primarily in this section, since they are more intuitive and capable to depict opposite results of the air masses wo.i.f. the examined European regions.

Three levels of [BC] (low: $< 300\,ng/m^3$, medium: 300–1000 ng/m^3 and high: $> 1000\,ng/m^3$) are defined as shown in Table 3. With regards to the probability of obtaining low [BC], the air masses w.i.f. NW and SE Europe had the highest and lowest probability of low [BC], respectively. Concerning the probability of reaching medium and high [BC], the air masses w.i.f. SE and NW Europe had the highest and lowest probability of medium and high [BC], respectively. Additionally, only the air masses w.i.f. SE Europe had a higher probability of high [BC] than the air masses wo.i.f. SE Europe, whereas the air masses w.i.f. NW, SW and NE Europe had a lower probability of high [BC] than the air masses wo.i.f. NW, SW and NE Europe, respectively. As a consequence, air masses that contained high [BC] at Hyltemossa station are largely due to the BC emissions from SE Europe.

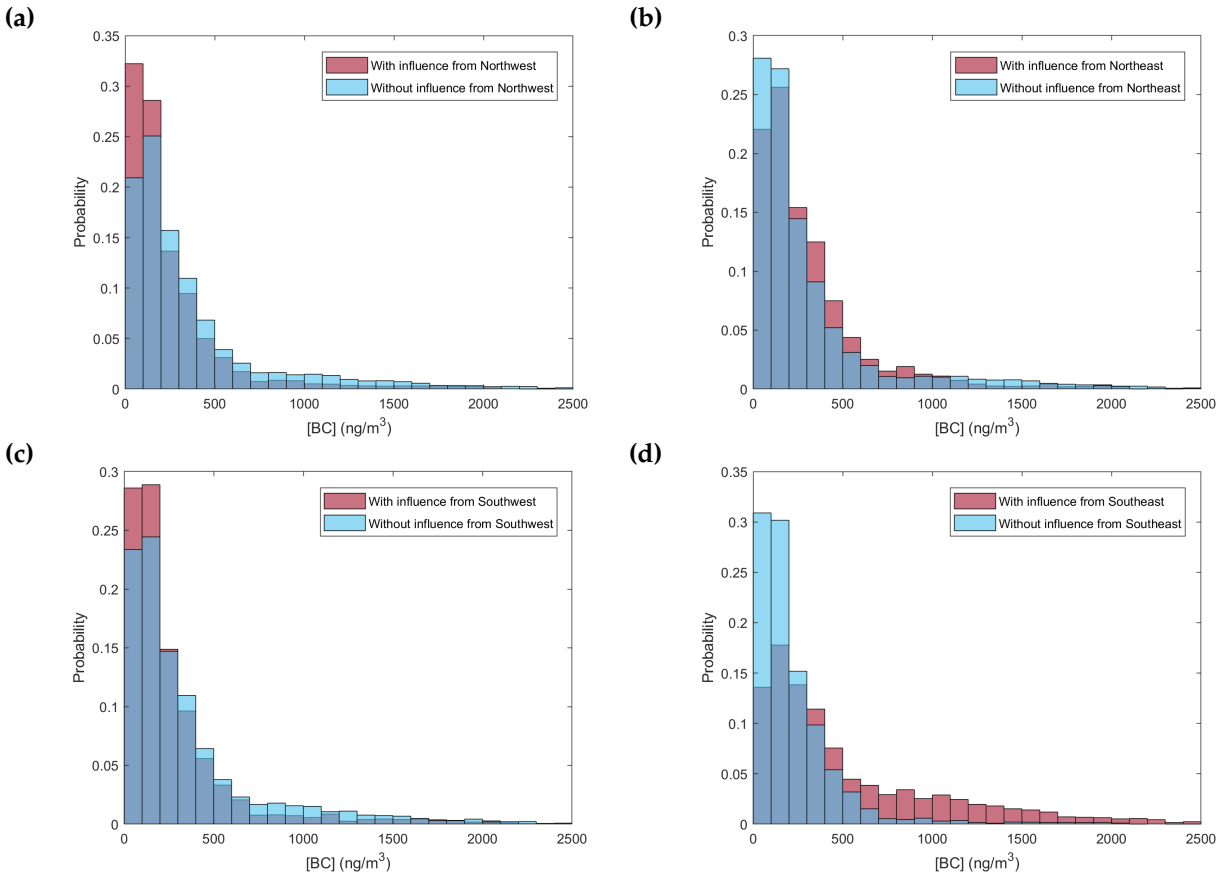

Figure 4: The probability of obtaining different values of [BC] at Hyltemossa station in 2018, in the conditions of the air masses with (red bins) and without (blue bins) influence from **(a)** NW, **(b)** NE, **(c)** SW, **(d)** SE Europe, respectively. Note that the unmentioned colour in the distributions is just a colour mixed instead of the probability of overlapping events.

Table 3: Tabulated data from Figure 4, which give the probability of obtaining low [BC] ($< 300\,\mathrm{ng/m^3}$), medium [BC] (300–1000 $\mathrm{ng/m^3}$) and high [BC] ($> 1000\,\mathrm{ng/m^3}$).

Conditions	Probability		
	Low [BC]	Medium [BC]	High [BC]
w.i.f. NE	0.6309	0.3160	0.05310
w.i.f. NW	0.7448	0.2176	0.03760
w.i.f. SE	0.4521	0.3621	0.1878
w.i.f. SW	0.7237	0.2288	0.04750
wo.i.f. NE	0.6974	0.2253	0.07730
wo.i.f. NW	0.6169	0.2893	0.09380
wo.i.f. SE	0.7624	0.2156	0.02200
wo.i.f. SW	0.6253	0.2851	0.08960

In summary, Figure 4 clearly depicts that the air masses w.i.f. Eastern Europe (i.e. NE and SE Europe) had a higher probability of obtaining medium and high [BC] at Hyltemossa via LDT than the air masses w.i.f. Western Europe (i.e. NW and SW Europe); the air masses w.i.f. Western Europe had a higher probability of attaining low [BC] than the air masses w.i.f. Eastern Europe. In other words, air mass trajectories that contained high [BC] tended to originate from Eastern Europe, while air masses with low [BC] tended to originate from Western Europe before arrival at Hyltemossa. The lowest [BC] was found in air masses that had spent time over NW Europe upwind Hyltemossa, whereas the highest [BC] was found in air masses that had spent time over SE Europe. Also, different meteorological conditions may affect the absolute [BC] in the air masses from different source regions, thus as the third task in the project the influence of precipitation on [BC] at Hyltemossa station was analysed.

Table 4: Geometric means of [BC] at Hyltemossa station in 2018, in the conditions of the air masses w.i.f. & wo.i.f. NE, NW, SE and SW Europe, respectively. Corresponding fraction of time and 95 % CI of the true geometric means of [BC] are also included.

Conditions	Fraction of time	$[BC]_{GM}$ (ng/m^3)	95 % CI (ng/m^3)
w.i.f. NE	0.3539	210.7319	203.7610–217.9414
w.i.f. NW	0.4453	158.7117	154.0099–163.5570
w.i.f. SE	0.2854	338.6670	324.9384–352.9756*
w.i.f. SW	0.4936	170.6658	165.7851–175.6902
wo.i.f. NE	0.6461	184.5882	179.6674–189.6437
wo.i.f. NW	0.5547	226.7597	220.3240–233.3833
wo.i.f. SE	0.7146	154.6807	151.2723–158.1660
wo.i.f. SW	0.5064	218.5805	212.0437–225.3189

* The CI should be interpreted with caution since the data of the air masses w.i.f. SE Europe could not be considered to be approximately normally distributed after applying the natural logarithm.

Table 4 shows that the air masses w.i.f. SE and NW Europe obtained the highest and lowest $[BC]_{GM}$, respectively. Basically, the air masses w.i.f. Eastern Europe recorded a higher $[BC]_{GM}$ than the air masses w.i.f. Western Europe. The results in Table 4 are consistent with the results in Figure 4 and Table 3. For instance, the air masses w.i.f. Eastern Europe had a higher probability of obtaining medium and high [BC] compared to the air masses w.i.f. Western Europe. Therefore, the air masses w.i.f. Eastern Europe reached a higher $[BC]_{GM}$ than the air masses w.i.f. Western Europe. Table 4 also shows the fraction of time

which Hyltemossa was influenced by air masses w.i.f. and wo.i.f. the different source regions. As an example, 35.39 % of the BC measurements in 2018 were sampled when the air masses had spend time over NE Europe at some time within the last 7-days upwind Hyltemossa station (w.i.f. NE Europe). The complementing results of the air masses wo.i.f. the examined European regions are also provided in Table 3 and 4.

3.2.3 Influence from local sources: Øresund

According to the definition in Table 1, Øresund includes the Danish capital, Copenhagen and the third-largest city in Sweden, Malmö. They are the closest large cities in the vicinity of Hyltemossa. Hence, Øresund is considered to be a sufficiently large urban region to potentially influence [BC] at Hyltemossa. In Figure 5 we compare the probability distribution of the air masses w.i.f. & wo.i.f. Øresund with the air masses w.i.f. & wo.i.f. Øresund and wo.i.f. Eastern Europe. Table 5 shows that the air masses w.i.f. & wo.i.f. Øresund (Figure 5a) had a probability difference of not greater than 0.0152 in all defined levels of [BC]. There is no statistically significant difference in $[BC]_{GM}$ when considering all air masses w.i.f. & wo.i.f. Øresund (Table 6).

However, Figure 5b shows that there was significant probability difference when the air masses which had spent time over Eastern Europe were removed. Compared to the air masses w.i.f. & wo.i.f. Øresund, the air masses w.i.f. & wo.i.f. Øresund and wo.i.f. Eastern Europe had a higher probability of low [BC] and lower probability of medium and high [BC], respectively. After the removal of the influence from Eastern Europe, the air masses w.i.f. Øresund had a lower (higher) probability of low (medium and high) [BC] than the air masses wo.i.f. Øresund by 0.1147 (0.08660 and 0.06170, respectively). Therefore, the air masses w.i.f. Øresund probably had a significant local [BC] contribution from Malmö and/or Copenhagen, but this is only evident if the LDT air masses from Eastern Europe, which generally had higher [BC] compared to Western Europe, is filtered out.

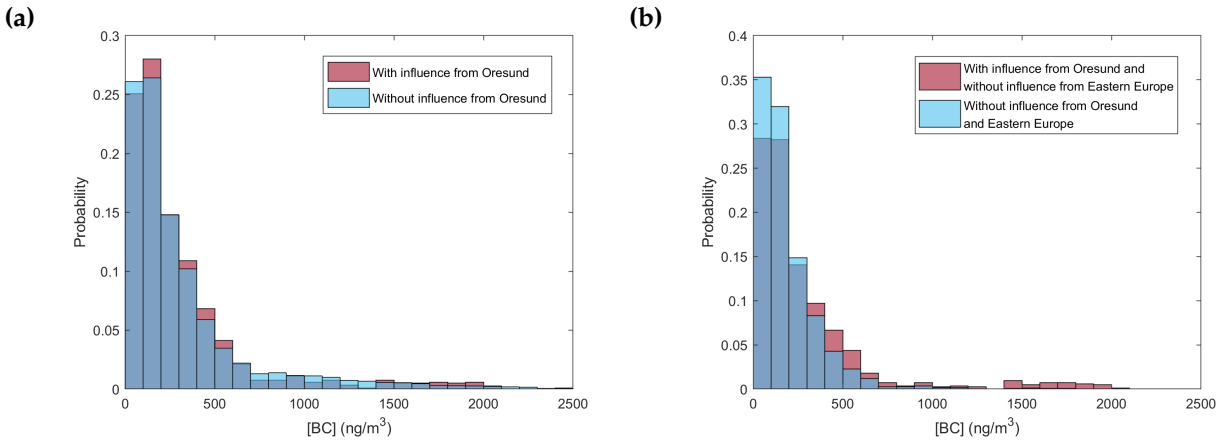

Figure 5: The probability of obtaining different values of [BC] at Hyltemossa station in 2018. Part **(a)** was in the conditions of the air masses with (red bins) and without (blue bins) influence from Øresund. Part **(b)** was in the conditions of the air masses with influence from Øresund and without influence from Eastern Europe (red bins) and without influence from Øresund and Eastern Europe (blue bins). Note that the unmentioned colour in the distributions is just a colour mixed instead of the probability of overlapping events.

Table 5: Tabulated data from Figure 5, which give the probability of obtaining low [BC] ($< 300\,\mathrm{ng/m^3}$), medium [BC] (300–1000 $\mathrm{ng/m^3}$) and high [BC] ($> 1000\,\mathrm{ng/m^3}$).

Conditions	Probability		
	Low [BC]	Medium [BC]	High [BC]
w.i.f. Øresund	0.6785	0.2658	0.05570
wo.i.f. Øresund	0.6731	0.2560	0.07090
w.i.f. Øresund and wo.i.f. Eastern Europe	0.7067	0.2436	0.04970
wo.i.f. Øresund and Eastern Europe	0.8214	0.1694	0.009200

Table 6: Geometric means of [BC] at Hyltemossa station in 2018, in the conditions of the air masses w.i.f. & wo.i.f. Øresund, and the air masses w.i.f. Øresund and wo.i.f. Eastern Europe & wo.i.f. Øresund and Eastern Europe, respectively. Corresponding fraction of time and 95 % CI of the true geometric means of [BC] are also included.

Conditions	Fraction of time	$[BC]_{GM}$ (ng/m^3)	95 % CI (ng/m^3)
w.i.f. Øresund	0.1360	188.7217	178.4557–199.5783
wo.i.f. Øresund	0.8640	194.2026	189.8121–198.6946
w.i.f. Øresund and wo.i.f. Eastern Europe	0.09470	172.2575	160.7885–184.5446*
wo.i.f. Øresund and Eastern Europe	0.3715	135.3962	131.4942–139.4140

* The CI should be interpreted with caution since the data of the air masses w.i.f. Øresund and wo.i.f. Eastern Europe could not be considered to be approximately normally distributed after applying the natural logarithm.

The local contribution to $[BC]_{GM}$ from Øresund was entirely changed if the influence from LDT (Eastern Europe) was ruled out. Table 6 shows that the air masses w.i.f. Øresund had a lower $[BC]_{GM}$ than the air masses wo.i.f. Øresund, but there was not a significant difference between them ($h = 0; p = 0.3155$). In converse, if the influence from Eastern Europe was not considered in the analysis, the air masses w.i.f Øresund had a higher $[BC]_{GM}$ than the air masses wo.i.f. Øresund, and there was a significant difference between them in this case ($h = 1; p < 0.0001$ on the assumption that the data were normally distributed). Moreover, the fraction of time of the air masses w.i.f. Øresund was decreased by 0.0413 (0.1360 compared to 0.09470) after eliminating the influence from Eastern Europe, which indicates that parts of the measurement data points were influenced by the air masses w.i.f. Eastern Europe. In the case of the air masses wo.i.f. Øresund, this effect was even greater (decreased by 0.4925 when 0.8640 compared to 0.3715). This could be the reason why the air masses wo.i.f. Øresund had a lower probability of low and medium [BC] than the air masses w.i.f. Øresund in Figure 5a and Table 5 (i.e. the air masses wo.i.f. Øresund were more often influenced by Eastern Europe than the air masses w.i.f. Øresund). As a result, it is likely that the air masses w.i.f. Øresund indeed had a local contribution to $[BC]_{GM}$ at Hyltemossa station, but it is necessary to withdraw the influence from LDT (Eastern Europe) when performing the local source analysis.

3.2.4 Influence from precipitation

As can be seen from Figure 6, $[BC]_{GM}$ at Hyltemossa station was influenced by different amount of precipitation. Each bar represents $[BC]_{GM}$ against the accumulated precipitation along the air mass trajectories during the last 6, 12, 24 and 48 h. In general, the estimated $[BC]_{GM}$ progressively decreased as the accumulated precipitation increased. Looking at the accumulated precipitation interval of $0 < x \leq 5\,\mathrm{mm/h}$, $[BC]_{GM}$ of the air masses during the last 6, 12, 24 and 48 h (all colours) recorded the most abrupt drop (averaged 21.46 % decrease). Although the accumulated precipitation along the trajectories during the last 6 h (blue) was never greater than 15 mm/h, its $[BC]_{GM}$ still had a descending trend in the first four intervals. Nonetheless, $[BC]_{GM}$ of the air masses during the last 12 h (yellow) in the accumulated precipitation intervals of $15 < x \leq 20$ and $x > 25\,\mathrm{mm/h}$ existed sudden growths, which was the only air masses that were not following the declining trend overall. This could be misleading because the error bar (which represents 95 % CI of the true geometric mean) in $15 < x \leq 25\,\mathrm{mm/h}$ was relatively large. Also, only one measurement was recorded in $x > 25\,\mathrm{mm/h}$, which basically could not be analysed in statistical ways (i.e. geometric mean and confidence interval of geometric mean). Otherwise, $[BC]_{GM}$ had a relatively steady decrease (averaged 14.65 % decrease excluding the air masses that during the last 12 h) from the accumulated precipitation intervals of $0 < x \leq 5$ to $x > 25\,\mathrm{mm/h}$.

In terms of the 95 % CI (error bars), $[BC]_{GM}$ of the air masses during the last 6, 12, 24 and 48 h (all colours) had significant differences in the first three intervals, respectively (Figure 6). However, there were no longer significant differences in the rest of the intervals because their corresponding error bars overlap. In principle, only the first three intervals could show the decreasing trend of $[BC]_{GM}$ against the accumulated precipitation statistically (averaged 21.15 % decrease).

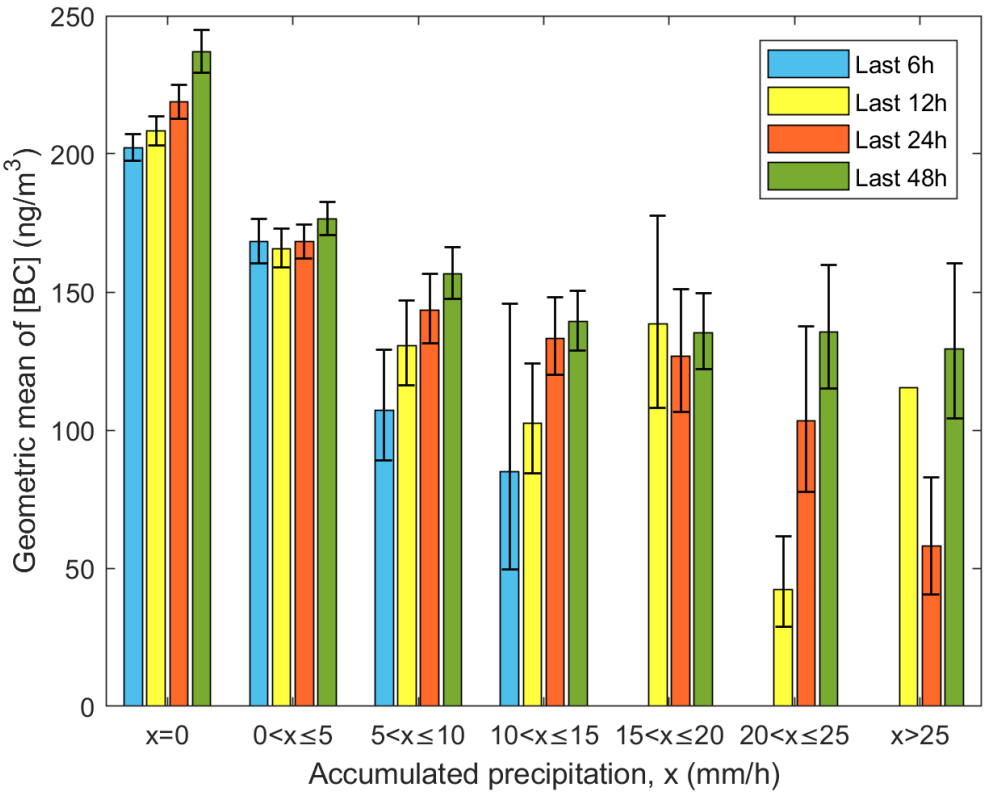

Figure 6: Relation between the geometric mean of [BC] and different intervals of accumulated precipitation x along the air mass trajectories during the last 6 (blue), 12 (yellow), 24 (orange) and 48 h (green) before arrival at Hyltemossa station in 2018. Error bars display 95 % CI of the true geometric mean of [BC].

Table 7 shows $[BC]_{GM}$ corresponding to the air masses w.i.f. & wo.i.f. precipitation during the last 6, 12, 24 and 48 h. In respect of the condition of w.i.f. precipitation, it is observed that the longer the time of accumulated precipitation along the trajectories, the greater the fraction of time, and vice versa for the condition of wo.i.f. precipitation. If the air masses did not have influence from precipitation for many hours (e.g. the air masses wo.i.f. precipitation during the last 48 h), $[BC]_{GM}$ had an ascending trend accordingly. However, if the air masses did have influence from precipitation, $[BC]_{GM}$ was not proportional to the last hours during which the air masses w.i.f. precipitation (e.g. the air masses w.i.f. precipitation during the last 6 h had the second most estimated $[BC]_{GM}$ in Table 7). This is not a surprising result since it is a combination of (1) having precipitation close to the station and (2) how much precipitation accumulated along the air mass trajectories. In case (1) more wet scavenging of BC should occur if the precipitation falls during the last 6 h compared to the precipitation falls during the last 12, 24 or 48 h. More BC emissions would probably take place in the latter case after the precipitation event upwind Hylte-

mossa which are not affected by precipitation. In case (2) the longer the last hours during which the accumulated precipitation along the air mass trajectories, the more accumulated precipitation (Table 8).

Table 7: Geometric means of [BC] at Hyltemossa station in 2018, in the conditions of the air masses w.i.f. & wo.i.f. precipitation during the last 6, 12, 24 and 48 h. Corresponding fraction of time and 95 % CI of the true geometric means of [BC] are also included.

Conditions	Fraction of time	$[BC]_{GM}$ (ng/m^3)	95 % CI (ng/m^3)
w.i.f. precip. (6 h)	0.2015	162.5762	155.0695–170.4463
w.i.f. precip. (12 h)	0.2713	158.4272	152.3846–164.7094
w.i.f. precip. (24 h)	0.3870	159.3721	154.3315–164.5773
w.i.f. precip. (48 h)	0.5608	165.3512	160.9788–169.8424
wo.i.f. precip. (6 h)	0.7985	202.1222	197.4142–206.9424
wo.i.f. precip. (12 h)	0.7287	208.3770	203.2435–213.6401
wo.i.f. precip. (24 h)	0.6130	218.6181	212.6991–224.7019
wo.i.f. precip. (48 h)	0.4392	236.3659	228.7210–244.2664

Table 8: Geometric means of the accumulated precipitation along the air mass trajectories during the last 6, 12, 24 and 48 h before arrival at Hyltemossa station in 2018.

During the last hours	Geo. mean of the accum. precip. (mm/h)
6 h	0.9972
12 h	1.2272
24 h	1.6941
48 h	2.4758

3.2.5 Local contribution to [BC] in Malmö and Copenhagen

The local contribution to [BC] in Malmö was estimated by comparing the Aethalometer data at Hyltemossa and Dalaplan station. Dalaplan station is situated in an important transport hub in Malmö and it is in the vicinity of Hyltemossa station. Dalaplan station is assumed to represent typical local street canyon [BC] levels in Malmö and Copenhagen, and under an approximate influence from LDT as Hyltemossa station. Dalaplan station archives in total 7967 hourly measurement data points in 2018, which give a data coverage of greater than 90 %. Table 9 shows the geometric means of [BC] at Hyltemossa and Dalaplan station in 2018, respectively. Under the assumptions above, the difference between the $[BC]_{GM}$ of Dalaplan and Hyltemossa station (183.7749 ng/m^3) was the estimated local contribution to [BC] at Dalaplan station.

Table 9: Geometric means of [BC] at Hyltemossa and Dalaplan station in 2018, respectively. Corresponding 95 % CI of the true geometric means of [BC] are also included.

Station	$[BC]_{GM}$ (ng/m^3)	95 % CI (ng/m^3)
Hyltemossa	193.4477	189.3958–197.5863
Dalaplan	377.2226	369.6338–384.9672

For the purpose of giving extra insights into information on local sources of BC, the diurnal (hourly) medians of [BC] in 2018 were analysed as well (Figure 7). At Dalaplan station, [BC] experienced a diurnal cycle with a pronounced growth (approximately 280 % rose) in the morning (05:00–09:00). This drastic increase in [BC] coincided with the morning traffic rush hour that generated BC from incomplete combustion of fossil fuel (e.g. within vehicle engines). After this period, [BC] gradually declined until the next cycle began. On the other side, Figure 7 does not capture a notable diurnal variation of [BC] at Hyltemossa station, which fluctuated between 170 and 216 ng/m^3 approximately. However, the small increasing trend of [BC] in the evening (18:00–23:00) possibly corresponded to local wood burning. Also, a low boundary layer height could explain higher [BC] in the evening if BC was from local sources. Both diurnal variations of [BC] at Dalaplan and Hyltemossa depict the local sources of BC at different times. On the whole, Figure 7 indicates that the local BC sources at Dalaplan station were larger than that at Hyltemossa station.

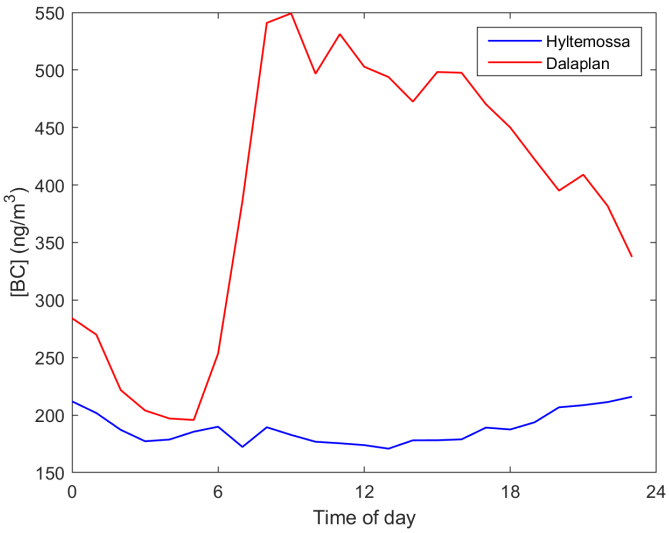

Figure 7: Diurnal variations of the median of [BC] at Hyltemossa and Dalaplan station in 2018, respectively.

4 Summary and conclusions

This thesis focused on analysing the measurement data estimated by the Aethalometer at Hyltemossa station by utilising the HYSPLIT model. Three types of influence on [BC] at Hyltemossa station during 2018 were analysed and investigated. At last, the local contribution to [BC] at Dalaplan station was estimated and compared with the [BC] at Hyltemossa station.

The first investigated influence on [BC] was from LDT air masses, which was estimated in terms of probability distributions and geometric means of [BC] for the air masses w.i.f. & wo.i.f. NW, NE, SW and SE Europe. Results of both probability distributions and geometric means agree that the air masses that contained relatively high [BC] at Hyltemossa station were very likely from Eastern Europe, since the air masses w.i.f. Eastern Europe had a higher probability of obtaining medium and high [BC] and thus reached a higher $[BC]_{GM}$ than that of Western Europe. In specific, SE was the largest contributor among four examined European regions to relatively high [BC] at Hyltemossa station through LDT.

The second investigated influence on [BC] at Hyltemossa station was from more local sources (namely the Øresund region), which was investigated by comparing the probability distributions and geometric means of [BC] for the air masses w.i.f. & wo.i.f. Øresund, and the air masses w.i.f. Øresund which excluded the influence from Eastern Europe. Results show that the air masses w.i.f. Øresund had a significant local contribution to [BC] ($h = 1; p < 0.0001$) after eliminating the influence from LDT (Eastern Europe).

The third investigated influence on [BC] was from precipitation, which was studied by plotting the relation between $[BC]_{GM}$ and different intervals of accumulated precipitation. $[BC]_{GM}$ for the air masses w.i.f. & wo.i.f. precipitation during the last 6, 12, 24 and 48 h upwind Hyltemossa were estimated as well. Results show that the estimated $[BC]_{GM}$ had a decreasing trend as the accumulated precipitation increased. Also, $[BC]_{GM}$ increased if the air masses did not have influence from precipitation for many hours. These confirm that the effect of precipitation on atmospheric aerosol particles (wet scavenging) is as expected also in the case of BC.

Lastly, the Aethalometer data at Dalaplan station in Malmö, which is assumed to be the typical [BC] contributor in Malmö and Copenhagen, was compared with that of Hylte-

mossa station. The difference between the $[BC]_{GM}$ of Dalaplan and Hyltemossa station estimated the local contribution to [BC] at Dalaplan station. The diurnal variations of [BC] at both stations were also demonstrated, which could indicate that the local BC sources at Dalaplan station were larger than that at Hyltemossa station.

5 Outlook

In the present [BC] analysis, three types of influence on [BC] was based on the air masses w.i.f. & wo.i.f. some regions or precipitation. A possible investigation in the future can be studying the time series of [BC], in order to have a better understanding of how the time spent over different source regions influence [BC] at Hyltemossa station. Furthermore, an analysis of BC emissions (e.g. based on the data retrieved from European Monitoring and Evaluation Programme) along each air mass trajectory could be performed, and thus evaluate whether there is a correlation between BC emissions and [BC]. Last but not least, there will also be a possibility to setup and run a chemistry transport model (e.g. ADCHEM) along the investigated air mass trajectories to determine which processes influence BC ageing downwind the urban regions.

6 Acknowledgements

First and foremost, I would like to thank my supervisor Pontus Roldin. Thank him for being very supportive and encouraging when I was confused, and proofreading this thesis. Pontus always listens to my thoughts and gives good advice. I could not have managed this thesis work without his valuable help. I would also like to thank Stina Ausmeel, Erik Ahlberg and Adam Kristensson for providing the Aethalometer data at Hyltemossa station, and Mårten Spanne for providing the Aethalometer data at Dalaplan station. A special thanks to my study advisor Elna Heimdal Nilsson who suggested a lot of possibilities of bachelor's project and introduced me to many teachers. Finally, I would like to thank my friends and family for their endless support.

7 References

Bond, T. C., Doherty, S. J., Fahey, D., Forster, P., Berntsen, T., DeAngelo, B., ... Koch, D. et al. (2013). Bounding the role of black carbon in the climate system: A scientific assessment. *Journal of Geophysical Research: Atmospheres*, *118*(11), 5380–5552.

Boucher, O., Randall, D., Artaxo, P., Bretherton, C., Feingold, G., Forster, P., ... Zhang, X. (2013). Clouds and aerosols. In T. F. Stocker, D. Qin, G.-K. Plattner, M. Tignor, S. K. Allen, J. Doschung, ...P. M. Midgley (Eds.), *Climate change 2013: The physical science basis. Contribution of Working Group I to the Fifth Assessment Report of the Intergovernmental Panel on Climate Change* (pp. 571–657). Cambridge UK, New York USA: Cambridge University Press.

Drinovec, L., Močnik, G., Zotter, P., Prévôt, A., Ruckstuhl, C., Coz, E., ... Wiedensohler, A. et al. (2015). The "dual-spot" Aethalometer: An improved measurement of aerosol black carbon with real-time loading compensation. *Atmospheric Measurement Techniques*, *8*(5), 1965–1979.

Hansen & Nazarenko, L. (2004). Soot climate forcing via snow and ice albedos. *Proceedings of the National Academy of Sciences*, *101*(2), 423–428.

Hansen & Schnell, R. (2005). The aethalometer. *Magee Scientific Company, Berkeley, California, USA*, 1–209.

Hinds, W. C. (1999). *Aerosol technology: Properties, behavior, and measurement of airborne particles*. John Wiley & Sons.

Jacob, D. J. (1999). *Introduction to atmospheric chemistry*. Princeton University Press.

Kuenen, J., Visschedijk, A., Jozwicka, M. & Denier Van Der Gon, H. (2014). TNO-MACC_II emission inventory; a multi-year (2003–2009) consistent high-resolution European emission inventory for air quality modelling. *Atmospheric Chemistry and Physics*, *14*(20), 10963–10976.

Löndahl, J. (2009). *Experimental Determination of the Deposition of Aerosol Particles in the Human Respiratory Tract* (Doctoral dissertation, Lund University).

Magee scientific. (2017). Aethalometer model AE33 user manual. *Ljubljana: Aerosol d.o.o.*

Martinsson, J., Abdul Azeem, H., Sporre, M. K., Bergström, R., Ahlberg, E., Öström, E., ... Eriksson Stenström, K. (2017). Carbonaceous aerosol source apportionment using the Aethalometer model–evaluation by radiocarbon and levoglucosan analysis at a rural background site in southern Sweden. *Atmospheric Chemistry and Physics*, *17*(6), 4265–4281.

Myhre, G., Shindell, D., Bréon, F.-M., Collins, W., Fuglestvedt, J., Huang, J., ... Zhang, H. (2013). Anthropogenic and natural radiative forcing. In T. F. Stocker, D. Qin, G.-K.

Plattner, M. Tignor, S. K. Allen, J. Doschung, ...P. M. Midgley (Eds.), *Climate change 2013: The physical science basis. contribution of working group i to the fifth assessment report of the intergovernmental panel on climate change* (pp. 659–740). Cambridge UK, New York USA: Cambridge University Press.

Stein, A., Draxler, R. R., Rolph, G. D., Stunder, B. J., Cohen, M. & Ngan, F. (2015). NOAA's HYSPLIT atmospheric transport and dispersion modeling system. *Bulletin of the American Meteorological Society*, *96*(12), 2059–2077.

Weingartner, E., Saathoff, H., Schnaiter, M., Streit, N., Bitnar, B. & Baltensperger, U. (2003). Absorption of light by soot particles: Determination of the absorption coefficient by means of aethalometers. *Journal of Aerosol Science*, *34*(10), 1445–1463.

World Health Organization. (2018). World health statistics 2018: Monitoring health for the SDGs, sustainable development goals.